Experimental Study of the Removal of Ground and Excited State Phosphorus Atoms by Atmospherically Relevant Species

Kevin M. Douglas[a*], Mark A. Blitz[a,b], Thomas P. Mangan[a], John M.C. Plane[a*]

[a]School of Chemistry, University of Leeds, Leeds, LS2 9JT, UK

[b]National Centre for Atmospheric Science (NCAS), University of Leeds, Leeds, LS2 9JT, UK

[*]Corresponding authors emails: K.M.Douglas@leeds.ac.uk; J.M.C.Plane@leeds.ac.uk

Abstract

The reaction kinetics of the ground and first two excited states of atomic phosphorus, P, with atmospherically relevant species, were studied at temperatures ranging from ~ 200 – 750 K, using a pulsed laser photolysis-laser induced fluorescence technique. The temperature dependence of the rate coefficients are parameterized as (units: cm^3 $molecule^{-1}$ s^{-1}, 1 σ errors):

$$k_{(P(^2P)+O_2)}\ (189 \le T/K \le 701) = (7.10 \pm 1.03) \times 10^{-12} \times (T/298)^{1.42 \pm 0.13} \times \exp^{((374 \pm 41)/T)}$$

$$k_{(P(^2D)+O_2)}\ (188 \le T/K \le 714) = (1.20 \pm 0.29) \times 10^{-11} \times (T/298)^{0.821 \pm 0.207} \times \exp^{((177 \pm 70)/T)}$$

$$k_{(P(^2D)+CO_2)}\ (296 \le T/K \le 748) = (5.68 \pm 0.36) \times 10^{-12} \times (T/298)^{0.800 \pm 0.103}$$

$$k_{(P(^2D)+N_2)}\ (188 \le T/K \le 748) = (1.42 \pm 0.03) \times 10^{-12} \times (T/298)^{1.36 \pm 0.04}$$

$$k_{(P(^4S)+O_2)}\ (187 \le T/K \le 732) = (3.08 \pm 0.31) \times 10^{-13} \times (T/298)^{2.24 \pm 0.29}$$

Electronic structure theory combined with RRKM calculations have been used to explain the unusual temperature dependence of $P(^4S) + O_2$. The small pre-exponential factor for the reaction results from a tight steric constraint, together with the requirement that the reaction occurs on doublet rather than sextet electronic surfaces.

1. Introduction

Phosphorus, P, is a key biological element with major roles in replication, information transfer, and metabolism.[1] Orthophosphate (oxidation state +5) is the dominant form of inorganic P at the Earth's surface; however, due to the low water solubility and reactivity of P(V) salts, they have a poor bio-availability. The low concentration of orthophosphate salts is also believed to be one of the major limiting factors for the development of life over long time scales.[2] In contrast, less oxidised forms of P (oxidation state ≤ +3) are far more bio-available. It has been suggested that these reduced forms of P may have originated from extra-terrestrial material that fell to Earth during the heavy bombardment period: previous studies have focused on the direct delivery of P to the surface in meteorites, to undergo processing through aqueous phase chemistry.[3] However, interplanetary dust contains around 0.8% P by elemental abundance,[4] and meteoric ablation in the 1 μbar region of a planetary upper atmosphere can

generate significant amounts of atomic P, which will then undergo atmospheric processing before deposition at the surface. The atmospheric chemistry of ablated P in the oxidizing atmospheres of the terrestrial planets, which is the subject of this paper, does not appear to have been investigated previously.

Most of the mass of extra-terrestrial P entering a planetary atmosphere is carried by interplanetary dust particles (IDPs) with a mass of ~ 5μg and a radius of ~ 100 μm.[5] A substantial fraction of these IDPs ablates due to aerobraking, at heights of ~ 80 km on Mars, 90 km on Earth, and 115 km on Venus.[6] The vaporized P atoms will then undergo chemical processing to form a variety of compounds, in which P may exist in different oxidation states due to the presence of both oxidizing and reducing agents in a planetary upper atmosphere. Figure 1 is a schematic diagram of the likely chemical pathways from P to either phosphonic (P oxidation state 3) or phosphoric acid (P oxidation state 5). This scheme has been constructed by performing high-level electronic structure calculations (at the CBS-QB3 level of theory [7]) of P species reacting with atmospherically relevant species to determine energetically viable reaction pathways. Initial oxidation of P is likely to proceed via reactions R1 and R2 to produce PO_2. From PO_2, an exothermic route to phosphoric acid exists via the formation of $HOPO_2$ (reactions R3 and 4). However, the bio-available compound H_3PO_3 should also form via HPO_2 (reactions R5 and 6):

	$\Delta H^{\circ}_{(0\ K)}$ (kJ mol^{-1})	
$P(^4S) + O_2 \rightarrow PO + O$	- 100	(R1)
$PO + O_2 \rightarrow PO_2 + O$	- 12	(R2)
$PO_2 + OH\ (+ M) \rightarrow HOPO_2$	- 441	(R3)
$HOPO_2 + H_2O\ (+ M) \rightarrow H_3PO_4$	- 188	(R4)
$PO_2 + H\ (+ M) \rightarrow HPO_2$	- 333	(R5)
$HPO_2 + H_2O\ (+ M) \rightarrow H_3PO_3$	- 173	(R6)

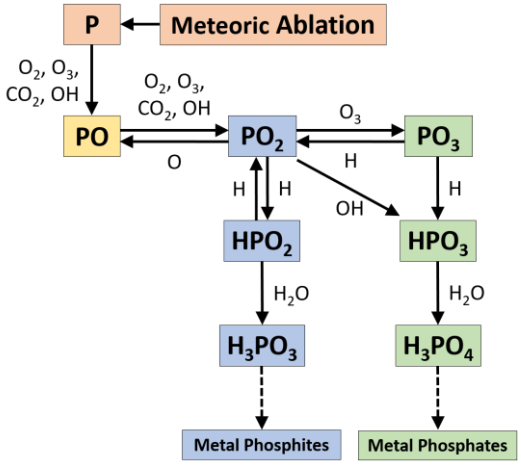

Figure 1. Proposed reaction scheme of the neutral chemistry of P in the upper atmosphere of a terrestrial planet.

Only two reactions from this scheme have been previously investigated (R1 and R2). However, no temperature dependences were determined, and for both reactions R1 and R2, the rate constants reported disagree by over an order of magnitude.[8-15] The poor characterization of the gas-phase chemistry of P may also reflect in the 3 order-of-magnitude difference between the observed and modelled abundances of PO in stellar outflows.[16]

In this paper, we present results from the first part of our investigation into the reactions of meteor-ablated phosphorus, reporting temperature-dependent coefficients for the reaction of ground state P(^{4}S) atoms with O_2. Rate coefficients were determined using a pulsed laser photolysis-laser induced fluorescence (PLP-LIF) technique, which we describe in Section 2. In addition, we also report rate coefficients for the removal of the first two excited states of phosphorus (the P(^{2}D) and the P(^{2}P) states) with atmospherically relevant species (reactions R7 – R12). We show that both of these states are formed in significant quantities following the PLP of the precursors PCl_3 and dimethyl methyphosphonate (DMMP).

			$\Delta H^\circ_{(0\ K)}$ (kJ mol^{-1})	
P(^{2}D) + O_2	→	PO + O	- 236	(R7a)
	→	P(^{4}S) + O_2	- 136	(R7b)
P(^{2}D) + CO_2	→	PO + CO	- 202	(R8a)
	→	P(^{4}S) + CO_2	- 136	(R8b)
P(^{2}D) + N_2	→	P(^{4}S) + N_2	- 136	(R9)
P(^{2}P) + O_2	→	PO + O	- 324	(R10a)
	→	P(^{2}D) + O_2	- 88	(R10b)
	→	P(^{4}S) + O_2	- 224	(R10c)
P(^{2}P) + CO_2	→	PO + CO	- 290	(R11a)
	→	P(^{2}D) + CO_2	- 88	(R11b)
	→	P(^{4}S) + CO_2	- 224	(R11c)
P(^{2}P) + N_2	→	P(^{2}D) + N_2	- 88	(R12a)
	→	P(^{4}S) + N_2	- 224	(R12b)

2. Experimental Procedure

The experimental apparatus employed in this study has been described in detail recently,[17-18] so only a brief synopsis is given here. All experiments were carried out in the slow flow reaction cell using the PLP-LIF technique, with detection of either the first or second excited state of P (the ^{2}D and ^{2}P states, respectively, hereafter collective referred to as P*), or of the PO molecule. The reaction cell consists of a cylindrical stainless steel chamber with four orthogonal horizontal arms and a fifth vertical side arm. The chamber was enclosed in a

thermally insulated container, which can be operated as a furnace or filled with dry ice, providing a temperature range from 190 – 800 K. Temperatures inside the reactor were monitored by a K-type thermocouple, placed at the centre of the chamber. The different radical precursors were introduced into the cell via one of the horizontal side arms as a dilute mixture of between 0.5 and 5 % in either N_2 or He (total precursor concentrations in the cell were typically much less than 0.1 %). The reagent and bath gases were combined in a mixing manifold prior to entering the chamber, and the mixture introduced through three different ports to allow homogeneous mixing in the central volume of the reactor where the reactions were initiated. Flow rates were controlled using calibrated mass flow controllers (MKS instruments), with total flow rates ranging from 100 – 400 standard cm^3 min^{-1}. These total flow rates were sufficient to ensure a fresh flow of gas into the cell for each photolysis laser pulse. The total pressure, as measured by calibrated capacitance manometers (Baratron MKS PR 4000) was controlled by a needle valve on the exit line to the pump. The photolysis and probe laser beams were introduced collinearly on opposite sides of the cell, and the fluorescence signal collected using a photomultiplier tube (Electron Tubes, model 9816QB) mounted orthogonally to the laser beams.

For reactions R1, and R7 – 12, P and P* atoms were produced by multiphoton dissociation of PCl_3 at 248 nm (R13). Some experiments were also carried out in which DMMP was used as a P atom precursor, as our investigation demonstrated that multiphoton dissociation of DMMP at 248 nm (R14) produced significant amounts of P*. The 248 nm light was generated from a KrF excimer laser (Lambda Physik COMPEX 102). The excimer beam was loosely focused using a 50 cm focal length lens, with the focal point positioned approximately 10 cm beyond the centre of the reaction chamber, giving a beam cross section in the interaction region of ~ 8 mm^2. Photolysis pulse energies of between 30 and 70 mJ/pulse were used.

$$PCl_3 + nh\nu \rightarrow P(^4S), P(^2D), P(^2P) + \text{co-products} \quad \text{(R13)}$$

$$DMMP + nh\nu \rightarrow PO, P(^4S), P(^2D), P(^2P) + \text{co-products} \quad \text{(R14)}$$

The LIF detection scheme used to monitor the first two excited states of P and the PO radical is shown in Table 1. The probe light was generated by frequency-doubling the output of a Nd:YAG pumped dye laser (a Quantel Q-smart 850 pumping a Sirah Cobra-Stretch with a BBO doubling crystal). The LIF signal was measured by the photomultiplier tube after passing through an appropriate interference filter (see Table 1), and recorded using a digital oscilloscope (LeCroy, LT262). The temporal evolution of the LIF signal was recorded by varying the time delay between the photolysis and probe lasers. A typical time-revolved LIF profile (Figure 2) consisted of 250 delay steps and resulted from the average of 5 individual delay scans.

Materials

He (99.999 %, BOC), N_2 (99.9995 %, BOC), O_2 (99.999 %, BOC), CO_2 (99.999 %, BOC) were used without further purification. PCl_3 (≥ 99.0 %, VWR), $POCl_3$ (99 %, Sigma Aldrich), and DMMP (97 %, Sigma Aldrich) were initially degassed by freeze-pump-thawing to remove volatile contaminants, and then made up as dilute vapours in N_2 or He.

Table 1. Transitions used for laser-induced fluorescence detection of the first two excited states of P and of PO.

Radical Species	Excitation λ (nm)[a]	Transition	Laser dye	Filter[b]
P(^{2}P)	253.6	$3s^23p^2(^3P)4s\ ^2P_{3/2} - 3s^23p^3\ ^2P°_{3/2}$	Coumarin 503	254 (8)
P(^{2}P)	215.4	$3s^23p^2(^1D)4s\ ^2D_{5/2} - 3s^23p^3\ ^2P°_{3/2}$	Exalite 428	216 (10)
P(^{2}D)	214.9	$3s^23p^2(^3P)4s\ ^2P_{1/2} - 3s^23p^3\ ^2D°_{3/2}$	Exalite 428	216 (10)
P(^{2}D)	213.6	$3s^23p^2(^3P)4s\ ^2P_{3/2} - 3s^23p^3\ ^2D°_{5/2}$	Exalite 428	216 (10)
PO	246.3	$A^2\Sigma^+ - X^2\Pi\ (v',v''\ 0,0)$[c]	Coumarin 503	254 (8)

[a] BBO frequency-doubling crystal employed. [b] Inerference filter peak transmission, FWHM in parentheses. [c] $A^2\Sigma^+ - X^2\Pi$ (v',v'' 0,0) transition pumped at 246.3 nm and the non-resonant (v',v'' 0,1) LIF monitored at 255.4 nm.[14]

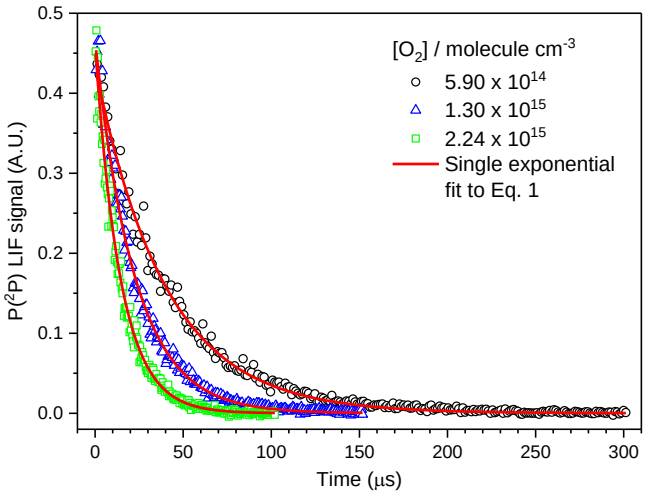

Figure 2. Decays of P(^{2}P) LIF signal (open symbols) at three different O_2 concentrations, together with a nonlinear least-squares fits of Equation E1 to the data (solid lines), at T = 380 K and a total pressure of 3.2 Torr.

3. Results

3.1 P(^{2}D) and P(^{2}P) removal

For both the first (^{2}D) and second (^{2}P) excited states of P, the LIF signal decayed exponentially with time (Figure 2), with no increase in the LIF signal observed even at very short probe-photolysis delay times. As all experiments were carried out under pseudo-first order conditions, such that the co-reagent, R, was in great excess of the radical species, the temporal evolution of P^* is given by:

$$[P^*]_t = [P^*]_0 e^{-k't} \qquad \text{(E1)}$$

where $[P^*]_0$ is the initial concentration of P^* from reaction R13, t is the time delay between the photolysis and probe laser pulses, and k' is the experimentally observed pseudo-first order loss rate, which is equal to:

$$k' = k_r[R] + k'_{loss} \quad \text{(E2)}$$

This expression encompasses the rates for all losses of P^*, including diffusion and removal by the precursor and bath gas (summed as k'_{loss}), and removal by the co-reagent, R. Equation E1 was fitted to the P^* profiles to extract the parameters $[P^*]_0$ and k'. A plot of k' vs [R] then yields a straight line with a slope equal to the bimolecular rate constant, k_r, and intercept k'_{loss}. Figure 2 shows typical examples of the temporal evolution of the LIF signals for $P(^2P)$ at three different O_2 concentrations, while Figure 3 illustrates bimolecular plots for reaction R7 at three different temperatures. The relatively small intercepts in Figure 3 demonstrate that loss of $P(^2P)$ is dominated by removal with the O_2 co-reagent.

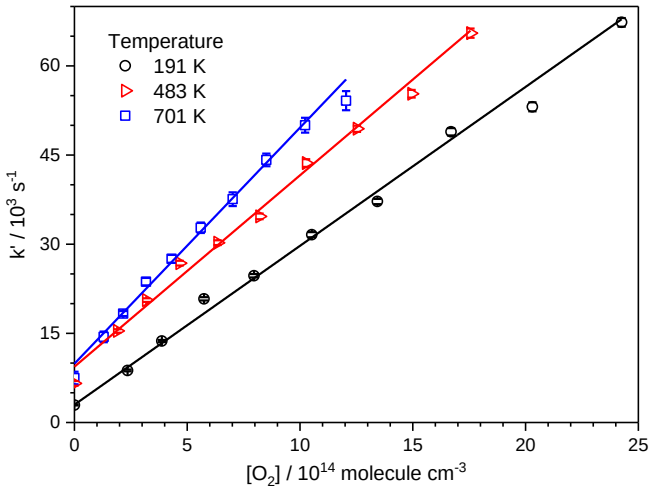

Figure 3. Bimolecular plots for the removal of $P(^2P)$ with O_2 at three different temperatures.

The bi-molecular rate coefficients for the removal of $P(^2P)$ with O_2, and for the removal of $P(^2D)$ with O_2, CO_2, and N_2, are presented in Table 2, and compared with available literature data in Figure 4. Errors reported are the 95 % confidence intervals of linear least squares fits of the pseudo first-order coefficients plotted as a function of co-reagent concentration. Additional details regarding the experimental conditions employed in each run are presented in Tables S1 – S4 of the Supporting Information (SI). No effects were observed on the bimolecular rate coefficients as pressure and radical concentration were varied by around a factor of 3, or when using different probe wavelengths. There has been only one previous investigation into the removal kinetics of P^* by various collision partners: Acuna, Husain, and Wiesenfeld used time-resolved atomic resonance absorption spectroscopy to study P* removal at room temperature.[19-20] In a similar method to that used in this study, P^* was produced by the pulsed photolytic irradiation of PCl_3 at short wavelengths ($\lambda > 160$ nm).

As can be seen in Figure 4, our room temperature result for P(^{2}P) with O_2 is in good agreement with that reported by Acuna, et al.[19] Looking at the temperature dependence of the reaction, we see typical Arrhenius behaviour at room temperature and above, with a small positive temperature dependence. However, below room temperature there is a small turnaround in the rate coefficient, with removal of P(^{2}P) at T ~ 191 K being slightly faster than at room temperature. The small k'_{loss} values obtained in these experiments indicate that quenching of the P(^{2}P) state by N_2 (R12) is a very minor process, for which we can only obtain a small upper limit of 5×10^{-14} cm^3 molecule^{-1} s^{-1}. The removal of P(^{2}P) by CO_2 was also investigated; however, we could only obtain an upper limit of the rate coefficient of 5×10^{-14} cm^3 molecule^{-1} s^{-1}, just below the value of $(7.3 \pm 1.9) \times 10^{-14}$ cm^3 molecule^{-1} s^{-1} determined by Acuna, et al.[20] The removal of P(^{2}P) with the PCl_3 precursor was also investigated at room temperature, for which we determined a rate coefficient of $(1.86 \pm 0.59) \times 10^{-11}$ cm^3 molecule^{-1} s^{-1}. This is significantly lower (by around a factor of 5) than the value of $(1.1 \pm 0.1) \times 10^{-10}$ reported by Acuna, et al.[19] The reason for this large discrepancy is unknown; however, it should be noted that the value we report is the average of three separate determinations using two different probe wavelengths.

For the reaction of P(^{2}D) with O_2, our room temperature value is around 50 % faster than that reported by Acuna, et al.[19] Looking at the temperature dependence of the reaction, as with the second excited state of P with O_2, we observe typical Arrhenius behaviour at room temperature and above. However, no change in the rate coefficient is observed as the temperature was lowered to 188 K, suggesting no turnaround in the rate coefficient at lower temperatures as was observed with P(^{2}P) with O_2, or that any turnaround occurs at temperatures below 188 K. For the reaction of P(^{2}D) with CO_2, our room temperature values are again higher than those of Acuna, et al.[20], by around 80 %. Looking at the temperature dependence of the removal of P(^{2}D) with CO_2, we again see typical Arrhenius behaviour at room temperature and above. We were unable to measure a removal rate for P(^{2}D) with CO_2 at T ~ 180 K, due to the CO_2 co-reagent freezing out in our reaction chamber at this temperature. We also measured the removal of P(^{2}D) with the PCl_3 precursor at room temperature, for which we obtained a rate coefficient of $(2.46 \pm 0.11) \times 10^{-10}$ cm^3 molecule^{-1} s^{-1}. This value is around 2.5 times higher than that value of $(9.7 \pm 0.9) \times 10^{-11}$ cm^3 molecule^{-1} s^{-1} reported by Acuna, et al.[19]

When measuring removal rates of P(^{2}D) with O_2 and CO_2, it was noted that the intercepts of the bimolecular plots, which relate to k'_{loss}, were significantly higher than those for the removal of P(^{2}P), or what would be expected for a diffusional loss rate (see Tables S1 – S3 in the SI). This implies that the P(^{2}D) state was being effectively quenched by the N_2 bath gas. Using the k'_{loss} values obtained in these experiments, we were able to determine rate coefficients for the removal of P(^{2}D) by N_2, by dividing k'_{loss} by the total concentration of N_2 used in each experiment. When doing this, a small correction to the k'_{loss} values was made to account for removal of P(^{2}D) by the precursor, using the room temperature rate determined in this study. This method yields rate coefficients for the removal of P(^{2}D) with N_2 over the temperature range of 188 – 748 K (Table S4). Comparing our room temperature rate for the removal of P(^{2}D) with N_2 to the upper limit of 5×10^{-16} cm^3 molecule^{-1} s^{-1} reported by Acuna, et al.[20], it can be seen that our value is around 3000 times larger, suggesting either a significant error in the previous study, or an error in our method of using k'_{loss} to determine the rate.

Therefore, to confirm the validity of our method for determining the removal rate of $P(^2D)$ with N_2, two additional experiments were carried out. In the first, we observed the removal of $P(^2D)$ as the total pressure of N_2 bath gas (and thus $[N_2]$) was varied. In this experiment the flows of N_2 and the precursor were adjusted to ensure the same $[PCl_3]$ despite changes in the pressure in the cell. In the second experiment, we again monitored the removal of $P(^2D)$ as we varied $[N_2]$, however in this case the total flow and pressure in the cell were kept constant by using helium as a make-up gas. These two additional experiments gave rate coefficients in excellent agreement with the two room temperature values determined using k'_{loss} values (Table S4), confirming the validity of this method for determining the removal of $P(^2D)$ with N_2.

Some experiments looking at the loss rates of $P(^2D)$ with O_2 and CO_2 that used helium as a bath gas also show high k'_{loss} values, when compared to the values seen for removal of $P(^2P)$ (Tables S1 to S3). This is the result of the faster removal of $P(^2D)$ by the PCl_3 precursor, compared with $P(^2P)$. Indeed, the k'_{loss} values obtained are consistent with the concentration of PCl_3 employed and the $P(^2D) + PCl_3$ rate coefficient determined.

The temperature dependences of the rate coefficients for the removal of P^* can be parameterised as follows (see dotted lines in Figure 4. Units: cm^3 $molecule^{-1}$ s^{-1}, 1 σ errors):

$$k_{(P(^2P)+O_2)}\ (189 \le T/K \le 701) = (7.10 \pm 1.03) \times 10^{-12} \times (T/298)^{1.42 \pm 0.13} \times \exp^{((374 \pm 41)/T)}$$

$$k_{(P(^2D)+O_2)}\ (188 \le T/K \le 714) = (1.20 \pm 0.29) \times 10^{-11} \times (T/298)^{0.821 \pm 0.207} \times \exp^{((177 \pm 70)/T)}$$

$$k_{(P(^2D)+CO_2)}\ (296 \le T/K \le 748) = (5.68 \pm 0.36) \times 10^{-13} \times (T/298)^{0.800 \pm 0.103}$$

$$k_{(P(^2D)+N_2)}\ (188 \le T/K \le 748) = (1.42 \pm 0.03) \times 10^{-12} \times (T/298)^{1.36 \pm 0.04}$$

Table 2. Rate coefficients for reactions R7-R10.

$P(^2P) + O_2$		$P(^2D) + O_2$		$P(^2D) + CO_2$		$P(^2D) + N_2$	
T (K)	k_r (10^{-11} cm^3 $molecule^{-1}$ s^{-1})	T (K)	k_r (10^{-11} cm^3 $molecule^{-1}$ s^{-1})	T (K)	k_r (10^{-12} cm^3 $molecule^{-1}$ s^{-1})	T (K)	k_r (10^{-12} cm^3 $molecule^{-1}$ s^{-1})
189	2.70 ± 0.22	188	2.09 ± 0.14	296	6.00 ± 0.25	188	0.72 ± 0.04
189	2.75 ± 0.21	295	2.06 ± 0.09	296	5.29 ± 0.30	295	1.38 ± 0.03
191	2.66 ± 0.15	295	1.96 ± 0.12	296	6.32 ± 0.17	295	1.39 ± 0.05
196	2.65 ± 0.17	296	2.12 ± 0.10	406	5.72 ± 0.43	296	1.39 ± 0.04
291	2.65 ± 0.27	296	1.95 ± 0.15	521	8.65 ± 0.35	296	1.46 ± 0.14
291	2.63 ± 0.23	296	2.20 ± 0.05	632	10.1 ± 0.5	386	2.21 ± 0.08
295	2.43 ± 0.07	386	2.15 ± 0.18	748	12.5 ± 0.4	406	2.52 ± 0.12
380	2.82 ± 0.17	491	2.43 ± 0.33			491	3.17 ± 0.22
483	3.18 ± 0.27	598	2.97 ± 0.24			521	3.20 ± 0.1
582	3.56 ± 0.27	714	3.18 ± 0.32			598	3.77 ± 0.12
701	3.97 ± 0.34					632	4.03 ± 0.17
						714	4.12 ± 0.23
						748	4.72 ± 0.13

Errors are the 95 % confidence intervals in the linear least squares fitting of the pseudo first-order coefficients as a function of co-reagent concentration.

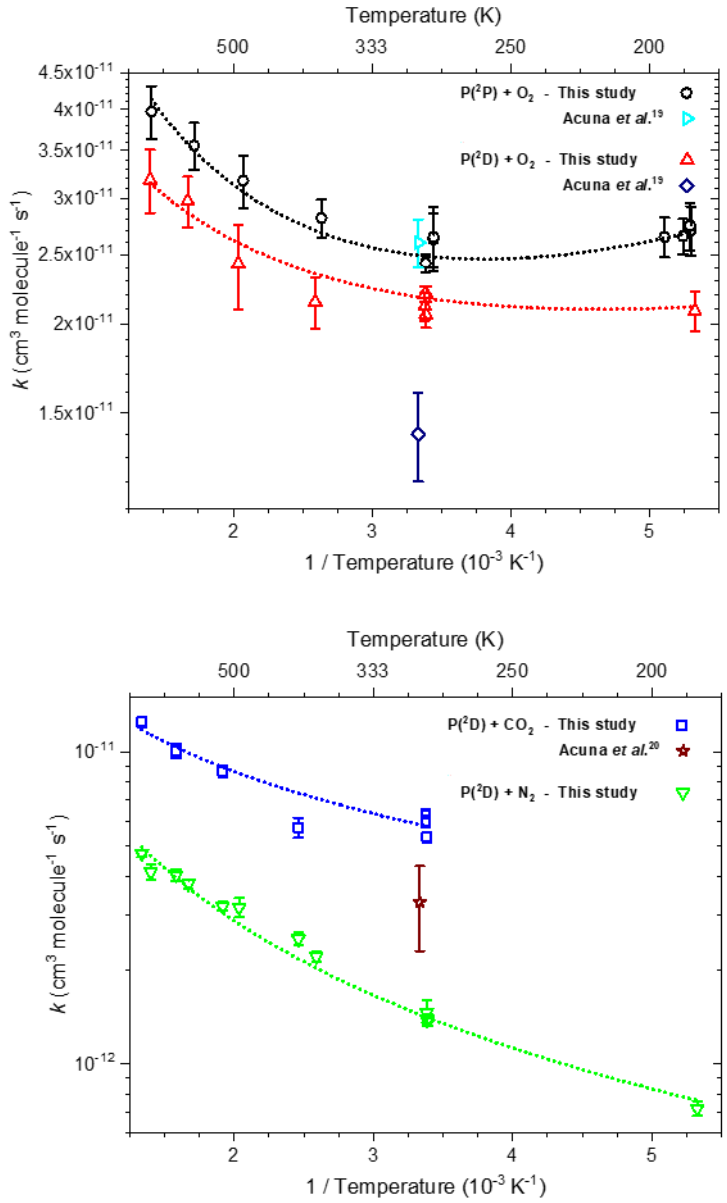

Figure 4. Temperature dependence of the rate coefficients for: Top panel. $P(^2P) + O_2$ – this study (black circles); Acuna, et al.[19] (turquoise triangle); and $P(^2D) + O_2$ – this study (red triangles); Acuna, et al.[19] (dark blue diamond). Bottom panel. $P(^2D) + CO_2$ – this study (blue squares); Acuna, et al.[20] (dark red star); $P(^2D) + N_2$ – this study (green triangles). Dotted lines are parameterized fits to the data provided by this study.

3.2 $P(^4S)$ removal

Initially we expected that following photolysis of PCl_3 in the presence of O_2, the following reactions would occur:

$$PCl_3 + nh\nu \rightarrow P(^4S) + Cl_x \text{ co-products} \quad \text{(R15)}$$

$$P(^4S) + O_2 \rightarrow PO + O \quad \text{(R1)}$$

$$PO + O_2 \rightarrow PO_2 + O \quad \text{(R2)}$$

Under pseudo-first order conditions (i.e. $[O_2]$ » $[P(^4S)]$ and [PO]), the PO LIF signal should be bi-exponential in nature, described by equation E3:

$$[PO]_t = \left(\frac{k'_{growth}}{k'_{removal} - k'_{growth}}\right)[P(^4S)]_0\left(e^{-k'_{growth}.t} - e^{-k'_{removal}.t}\right) \qquad (E3)$$

where k'_{growth} and $k'_{removal}$ are the pseudo first-order rate coefficients for reactions R1 and R2, and $[P(^4S)]_0$ is the initial amount of $P(^4S)$ formed following photolysis of PCl_3. Plots of k'_{growth} and $k'_{removal}$ vs $[O_2]$ should then be linear with slopes equal to the bimolecular rate coefficient for reactions R1 and R2, and intercepts k'_{loss} (Equation E2). Initial experiments monitoring the PO LIF signal did produce profiles that appeared to be bi-exponential in nature (Figure 5), and the parameters k'_{growth}, $k'_{removal}$, and $[P(^4S)]_0$ were obtained by fitting equation E3 to the data. It should be noted when analysing these bi-exponential PO profiles, that if the reaction forming PO is faster than the reaction removing PO (i.e. R1 is faster than R2), then a growth and loss profile of the PO LIF signal such as that in Figure 5 will be observed, in which the growth rate (k'_{growth}) in the early part of the profile is governed by the formation of PO (reaction R1), while the loss rate ($k'_{removal}$) in the tail end of the profile is governed by the removal of PO (reaction R2). However, if the reaction forming PO is now slower than the reaction removing it (i.e. R1 is slower than R2), then a bi-exponential profile will still be observed (albeit with lower absolute signal), except that k'_{growth} in the early part of the profile is governed by the fast removal of PO (reaction R2), while $k'_{removal}$ in the tail end of the profile is governed by the slow formation of PO (reaction R1). Therefore, to be able to assign whether k'_{growth} or $k'_{removal}$ is related to R1 or R2, knowledge of which reaction is faster is required.

There are significant discrepancies in the literature over the rate coefficients of both reaction R1 and R2. For the reaction between $P(^4S)$ and O_2, there have been four previous room temperature determinations: Husain and Norris[11] and Husain and Slater[12] found $k_1 \sim 2.0 \times 10^{-12}$ cm^3 $molecule^{-1}$ s^{-1}, while Clyne and Ono[9] and Henshaw, et al.[10] measured $k_1 \sim 1.0 \times 10^{-13}$ cm^3 $molecule^{-1}$ s^{-1} i.e. a factor of 20 times smaller. The lower values provided by the two more recent studies were both obtained using VUV resonance fluorescence detection of ground state $P(^4S)$ atoms in a discharge-flow system, with the $P(^4S)$ atoms formed by passing diluted PCl_3 and/or PBr_3 through a radio-frequency discharge. The higher values obtained in the two earlier studies employed repetitive pulsed irradiation of PCl_3 to produce $P(^4S)$ atoms, the temporal evolution of which were monitored by either attenuation of atomic resonance radiation in the VUV,[11] or as in the two later studies, by VUV resonance fluorescence.[12] The large discrepancy between the four studies is discussed by Clyne and Ono[9]. They suggested that the larger concentrations of PCl_3 precursor used in the earlier studies, coupled with the flash photolysis technique, produced significant amounts of secondary dissociation products (such as PCl_2, PCl, Cl, and Cl_2) relative to $P(^4S)$ atoms, when compared to the RF discharge technique and lower PCl_3 concentrations employed in the two more recent studies. These secondary products may have influenced the kinetics of the $P(^4S) + O_2$ reaction, particularly if significant amounts of secondary Cl_2 were formed. This is because the rate of $P(^4S)$ with Cl_2 has been shown to be significantly faster than the rate with O_2 by both Husain and Slater[12] and Clyne and Ono[9], although again both studies disagree significantly on the absolute value of the $P(^4S) + Cl_2$ rate. As a consequence, Clyne and Ono[9] were careful to minimise the possible effects of these secondary dissociation products. Indeed, no significant change in $P(^4S)$ depletion rates was

found when substituting PBr_3 for PCl_3 as the source of P atoms, suggesting the effect of any secondary products in this later study to be minor. For these reasons, we expected the value for k_1 to lie at the lower end of the range i.e. close to the value of ~ 1.0×10^{-13} cm^3 $molecule^{-1}$ s^{-1} found by Clyne and Ono[9] and Henshaw, et al.[10].

For the reaction between PO and O_2 (R2), there have also been four previous room temperature determinations of k_2; Aleksandrov, et al.[8] and Wong, et al.[15] measured $k_2 \sim 2 \times 10^{-13}$ cm^3 $molecule^{-1}$ s^{-1}, while Long, et al.[13] and Sausa, et al.[14] found that $k_2 \sim 1.3 \times 10^{-11}$ cm^3 $molecule^{-1}$ s^{-1} i.e. 60 times faster. The lower values were obtained from fast flow tube studies, using a microwave discharge of DMMP to produce PO, the loss of which was then monitored using LIF. Both studies have significant uncertainties (of around a factor of 2) arising from uncertainties in the flow rates. The two larger rate coefficients were measured using PLP of DMMP to produce PO, the loss of which was again monitored by LIF. In the study by Sausa, et al.[14], a KrF excimer laser (248 nm) was used as a photolysis source. As is discussed in their paper, it is possible that the focused KrF radiation may result in the dissociation of O_2, so that they observe the reaction of PO + O atoms rather than PO + O_2. Indeed, they noted a significant deviation from exponential decay of PO when the photolysis source was switched to a shorter wavelength ArF laser (193 nm), which is well known to generate O atoms. However, interference from O atoms can in fact be ruled out: in the study by Long, et al.[13] in which PO was produced from the infrared multiphoton dissociation of DMMP, a method which cannot generate O atoms from O_2, a bimolecular rate constant for k_2 was obtained in good agreement with that from the KrF laser study.[14] Another possible cause of the discrepancy between the laser photolysis vs flow tube experiments may lie in the time scales of the experiments. While the laser photolysis studies occur on a microsecond timescale, the flow discharge experiments occur on the scale of milliseconds. The comparatively fast rate for reaction R2 (PO + O_2 → PO_2 + O) as measured by Long, et al.[13] and Sausa, et al.[14] implies a relatively low reaction barrier. This, coupled with the near thermo-neutrality of the reaction (ΔH = -12 kJ mol^{-1} at the CBS-QB3 level of theory) suggests that an equilibrium between the forward and reverse reactions might be reached in experiments where there is a long contact time between the reactants, such as the flow discharge experiments. This problem would be compounded by the probable presence of O atoms in the flow discharge experiments. For these reasons we consider that k_2 lies closer to the value of 1.3×10^{-11} cm^3 $molecule^{-1}$ s^{-1} obtained by Long, et al.[13] and Sausa, et al.[14]

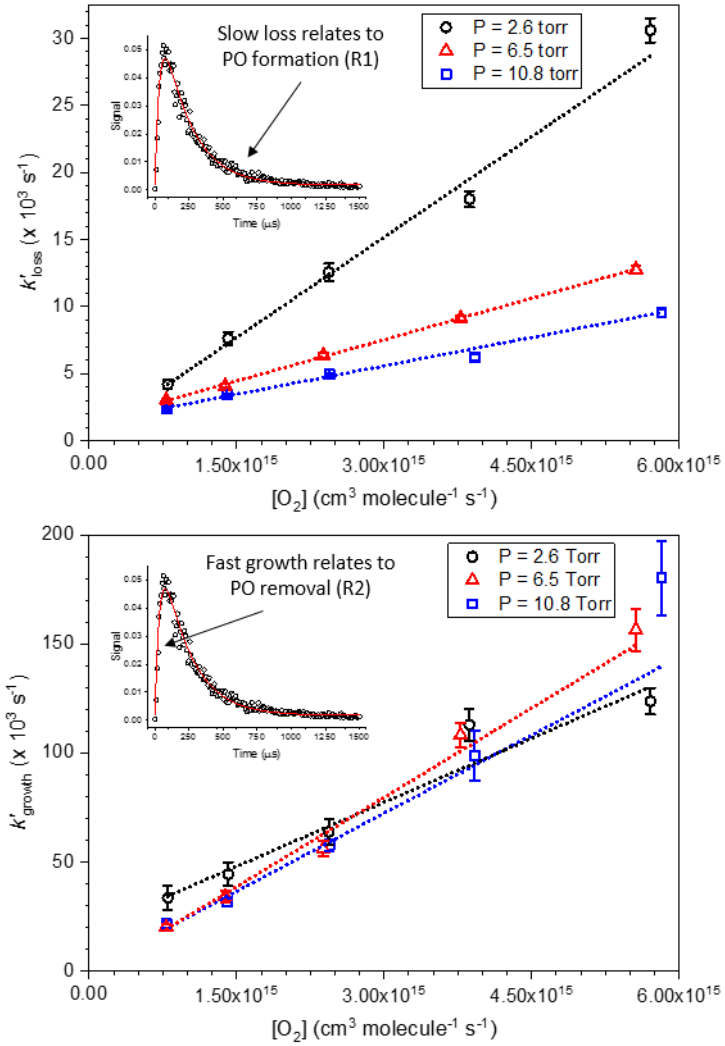

Figure 5. Bimolecular plots for the formation (upper panel) and removal (lower panel) of PO following PLP of PCl_3 in the presence of O_2 at a temperature of T = 392 K, at three different pressures (black circles; P = 2.6 Torr, red triangles; P = 6.5 Torr, blue squares; P = 10.8 Torr). Insets show the apparent biexponential behaviour of the PO LIF profiles. As the reaction forming PO (R1) is slower than the reaction removing PO (R16), changes in the fast growth of the PO signal relate to the fast PO removal via R2, while changes in the slow loss of PO signal relate to the slow formation of PO via R1 (see text for details).

From this review of the literature we conclude that $k_1 << k_2$,which means that in the PO profiles obtained following PLP of PCl_3 in the presence of O_2, the growth in signal in the early part of the profile relates to the removal of PO by R2, while the loss of signal at the tail end of the profile relates to the slow formation of PO from R1. Initial experiments monitoring the PO LIF signal following PLP of PCl_3 in the presence of O_2 were conducted over a range of temperatures and pressures. Figure 5 shows a typical example of the apparent bi-exponential nature of the PO LIF signal, as well as bimolecular plots for the formation and removal

reactions of PO at three different pressures. Inspection of Figure 5 shows that the rate of formation of PO decreases with increasing pressure, while the rate of removal of PO remains relatively constant as P is varied. This pressure dependence was observed over the temperature range investigated (295 – 720 K). This inverse pressure dependence on the rate of formation of PO is a surprising result, which can be attributed to the presence of the two reactive low-lying metastable ^{2}P and ^{2}D states of P. As the reactions of these states with O_2 are faster than for P(^{4}S), PO is formed faster, giving an inflated rate to reaction R1. At higher bath gas pressures, these excited states are more effectively quenched, resulting in a rate of PO formation that more closely resembles the P(^{4}S) + O_2 rate. Therefore, in order to measure the true rate of reaction between P(^{4}S) and O_2, experiments were carried out at higher bath gas pressures and with high [O_2]. In these experiments, any P* formed would be rapidly removed, either by collisional quenching by the bath gas, or by reaction with O_2. This would appear as a fast growth and loss of PO LIF signal. Any ground state P(^{4}S) formed would then react with O_2 on a much longer timescale; this slow formation of PO would appear as a slow decay of the PO LIF signal. A typical PO LIF profile obtained at a high bath gas pressure (~ 20 Torr) and high [O_2] is shown in Figure 6, in which the fast growth and loss of the PO LIF signal, together with the slow decay on a longer timescale, is clearly visible. As these experiments are carried out under pseudo first-order conditions, the tail end of the PO LIF signal can be fitted to a single exponential:

$$[\mathrm{PO}]_t = [\mathrm{P}(^4\mathrm{S})]_0 e^{-k'.t} \qquad \text{(E4)}$$

where [P(^{4}S)]$_0$ is the initial concentration of P(^{4}S), formed either directly from the photolysis of PCl_3, or from the fast quenching of excited state P*, t is the time delay between the photolysis and probe laser pulses, and k' is the experimentally observed pseudo-first order rate for reaction the reaction of P(^{4}S) with O_2 (R1). A plot of k' vs [O_2] then yields a straight line with a slope equal to the bimolecular rate constant for reaction R1 (inset in Figure 6). The temperature dependence of k_1 can be parameterised as follows (cm^3 molecule^{-1} s^{-1}, 1 σ errors):

$$k_{(\mathrm{P}(^4\mathrm{S})+\mathrm{O}_2)}\ (187 \leq \mathrm{T/K} \leq 732) = (3.08 \pm 0.31) \times 10^{-13} \times (\mathrm{T}/298)^{2.24 \pm 0.29}$$

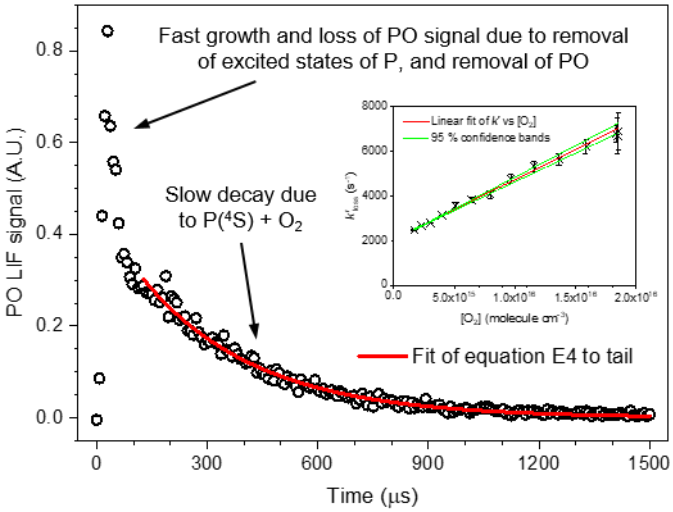

Figure 6. PO LIF signal following PLP of PCl_3 at a total pressure of 20.6 Torr and $[O_2]$ = 3.97 × 10^{15} molecule cm^{-3}, at T = 291 K. Inset shows a bimolecular plot for reaction R1 at T = 291 K, giving k_1 = (2.70 ± 0.12) × 10^{-13} cm^3 $molecule^{-1}$ s^{-1}.

Table 3. Rate coefficients for $P(^4S) + O_2$.

T (K)	k_r (10^{-13} cm^3 $molecule^{-1}$ s^{-1})
187	1.42 ± 0.18
291	2.70 ± 0.12
295*[a]	1.1 ± 0.2
293*[b]	0.99 ± 0.04
300*[c]	(2.1 ± 0.6) × 10^{-12}
300*[d]	(2.0 ± 0.2) × 10^{-12}
393	7.75 ± 0.79
481	11.5 ± 0.9
583	16.4 ± 1.7
732	14.0 ± 2.8

Errors are the 95 % confidence intervals in the linear least squares fitting of the pseudo first-order coefficients as a function of co-reagent concentration. * Literature values taken from: [a] Henshaw, et al.[10]; [b] Clyne and Ono[9]; [c] Husain and Slater[12]; [d] Husain and Norris[11].

4. Discussion

4.1 Comparison with previous work

The bimolecular rate coefficients for the reaction of P(^{4}S) with O_2 (R1) determined in this study are compared with the literature values in Table 3 and Figure 8. Additional details regarding the experimental conditions employed in each run are presented in Table S5 of the Supporting Information (SI). The room temperature value determined in this study is around 2.5 times larger than the values presented by Clyne and Ono[9] and Henshaw, et al.[10], and around 8 times smaller than the values presented by Husain and Norris[11] and Husain and Slater[12]. As discussed previously, Clyne and Ono[9] suggested the discrepancy between the measured rates of reaction R1 may be due to interference from secondary photolysis products in the earlier studies by Husain, the result of the (relatively) high precursor concentrations employed in their studies (~10^{14} molecule cm^3 compared to ~10^{12} molecule cm^3 in the later studies). However, the room temperature rate determined in this study is closer to the lower values of the later studies, despite using PCl_3 precursor concentrations (~ 6×10^{13} molecule cm^3) which are towards the higher end of those employed in the literature. This implies that interference from secondary photolysis products is not a significant problem.

The other possible source of error in measurements of k_1 is interference from P*, which has not been discussed in the previous studies. As our study shows, photolysis of a range of phosphorus precursors produces substantial amounts of P*, which can react with O_2 to form PO, or be relaxed down to ground state P(^{4}S). All four previous studies have determined k_1 by monitoring the removal of P(^{4}S) in the presence of O_2. If in these experiments P* are being relaxed down to the ground P(^{4}S) state, the observed removal would be slower, resulting in a smaller rate coefficient for the reaction. This is not expected to be a problem for the earlier two studies [11-12], in which higher bath gas pressures, precursor concentrations, and [O_2] mean that the majority of any P* formed should have been removed before monitoring of P(^{4}S) started (due to gating of the photomultiplier tube in those experiments). However, in the latter two studies, in which a similar delay between data acquisition and the initiation of the reaction is employed (~ 200 μs), the lower bath gas pressures, precursor concentrations, and [O_2] employed would mean that any P* formed would be removed on the timescale of the experiment, which could result in an underestimate of the rate coefficient. Indeed, the room temperature rate coefficients reported by the latter two studies are significantly smaller than that determined in the present study.

In our experiments, where the rate of the reaction of P(^{4}S) with O_2 was measured by monitoring the formation of the PO product, we ensured that P* removal occurs on a much faster time scale than the slow production of PO from reaction 1 was observed. For example, even at the lowest [O_2] used in our experiments (~ 2×10^{15} molecule cm^3), > 99 % of P* would be removed within 120 μs, using k(P(^{2}D) + O_2) = 2×10^{-11} cm^3 molecule^{-1} s^{-1} at T = 298 K. The rate of P(^{2}P) with O_2 is even faster. This ensured that production of PO from P* + O_2 did not inflate our removal rate, or that formation of P(^{4}S) from quenching of P* reduce the removal rate of P(^{4}S) at the longer reaction times where k_1 was determined.

4.2 Theoretical Calculations

In order to understand the unusual kinetic behaviour of the reaction between P(^{4}S) and O_2, and also to extrapolate to conditions relevant for planetary atmospheres, electronic structure calculations were combined with Rice-Ramsperger-Kassel-Markus (RRKM) theory. The hybrid density functional/Hartree−Fock B3LYP method was employed from within the Gaussian 16 suite of programs,[7] combined with Dunning's quadruple-ζ aug-cc-pVQZ correlation consistent basis, augmented with diffuse functions.[21] Molecular geometries were first optimized and checked for wave function stability, and their respective vibrational frequencies were calculated. The resulting geometries, rotational constants, vibrational frequencies and energies with respect to P(^{4}S) + O_2 are listed in Table 4. The resulting potential energy surface is illustrated in Figure 7, which also depicts the geometries of the stationary points.

For the RRKM calculations, the Master Equation Solver for Multi-Energy well Reactions (MESMER) program[22] was used. The reaction is assumed to proceed via the formation of an excited P-OO adduct, which can either dissociate back to P + O_2 or forward to OPO, before dissociating to the PO + O product. Stabilization by collision with the N_2 third body into either the P-OO or the relatively deep OPO well can also occur. The internal energy of the adduct is divided into a contiguous set of grains (width 200 cm^{-1}), each containing a bundle of rovibrational states. Each grain is then assigned a set of microcanonical rate coefficients for dissociation back to the reactants or to the products, using inverse Laplace transformation to link them directly to the high-pressure limiting recombination coefficients. In the case of P + O_2, an Arrhenius expression was optimised to give the best fit of the RRKM model to the experimental data, yielding k_∞(P + O_2) = 4.4×10^{-12} exp$^{(-720/T)}$ cm^3 molecule^{-1} s^{-1}. For PO + O, k_∞(PO + O) was set to 1.0×10^{-10} exp$^{(-25/T)}$ cm^3 molecule^{-1} s^{-1} i.e. a typical capture rate coefficient with a small positive temperature dependence. The calculated rate coefficient for P + O_2 is not sensitive to k_∞(PO + O) unless it is reduced by a factor of more than 100. The probability of collisional transfer between grains was estimated using the exponential down model: the average energy for downward transitions $\langle \Delta E \rangle_{down}$ was set to 300 cm^{-1}, typical of M = N_2 at 300 K, with a $T^{0.25}$ temperature dependence.[23]

Figure 8 illustrates a satisfactory fit to the experimental data from this study. There is a negligible pressure dependence to the reaction even up to 106 Torr (at 300 K), because the transition state between P-OO and OPO is 66 kJ mol^{-1} below the entrance channel, and the exit channel to PO + O is 84 kJ mol^{-1} exothermic. Indeed, the RRKM calculations suggest a pressure of 4000 bar (at 300 K) would be required for OPO to form 50 % of the products via collisional stabilization. What is interesting is the small pre-exponential factor and activation energy in the fit of k_∞(P + O_2) to the experimental data (see above). There are two reasons for the small pre-exponential factor. First, there is a tight steric constraint: Figure 9 illustrates the doublet potential energy surface for the approach of P to O_2, as a function of P-OO distance and P-O-O angle. This shows that for the barrier to form the P-OO intermediate to be lower than 10 kJ mol^{-1}, the P-O-O approach angle is limited to between 105 and 125^o. Second, the combination of P(^{4}S) and O_2($^3\Sigma_g^-$) generates surfaces of both doublet and sextet spin multiplicity. However,

the sextet surfaces are repulsive which further reduces the probability of successful reaction by a factor of ~2.

The temperature dependence for the reaction is predicted to be:

$$k_{(P(^4S)+O_2)}\ (150 \leq T/K \leq 1400) = 4.20 \times 10^{-12} \times \exp^{(-600/T)}\ cm^3\ molecule^{-1}\ s^{-1}.$$

4.2 Atmospheric Implications

Meteoric ablation of IDPs entering the upper atmosphere of a terrestrial planet occurs at around the 1μbar region.[6] Phosphorus will likely ablate from these particles as P, PO and PO_2,but hyperthermal collisions with atmospheric molecules will immediately dissociate the molecules to P and P*. P^+ ions are also likely to form during ablation, but these react rapidly with O_2 and CO_2 to yield PO^+,[24] which will then undergo dissociative recombination with electrons to yield P and P*. In the Earth's atmosphere at the ablation peak around 85 km,[6] P* will be rapidly removed by collisions with O_2: the $P(^2P)$ state will have an e-folding lifetime of around 1.2 ms, while the $P(^2D)$ state will have a lifetime of ~1.4 ms, with almost 90 % of $P(^2D)$ removed by O_2 rather than N_2. Ground state $P(^4S)$ atoms will survive somewhat longer with a lifetime against oxidation by O_2 of around 280 ms. The resulting PO will in turn be oxidized by O_2 to PO_2. Note that because there is around 10^5 times more O_2 than O_3 at this altitude,[25] oxidation by O_3 is not significant. As there are no exothermic processes to convert PO or PO_2 back to P, the speciation of phosphorus will depend only on reactions converting PO_2 into HOPO, HPO_2 and $HOPO_2$, as shown in Figure 1.

Table 4. Molecular properties of the stationary points on the doublet potential energy surface for $P(^4S) + O_2$ (illustrated in Figure 7).

Molecule	Geometry (Cartesian co-ordinates in Å) [a]	Rotational constants (GHz) [a]	Vibrational frequencies (cm^{-1}) [a]	E(0 K) (kJ mol^{-1}) [b]
TS1 (from $P + O_2$ to P-OO	P, 0.002, 0., 0.009 O, 0.002, 0., 2.531 O, 1.058, 0., 3.134	76.364 3.7430 3.5681	121i, 225, 1497	3.1
P-OO	P, -0.267, 0. , -0.122 O, 0.257, 0., 1.415 O, 1.558, 0., 1.729	90.083 6.6848 6.2231	259, 671, 1016	-97.3
TS2 (from P-OO to OPO)	P, -0.623, -0.544, 0. O, 0, -0.033, 0.862, 0. O, 1.387, 0.181, 0.	34.713 10.162 7.8608	-341i, 392, 1103	-66.2
OPO	P, 0.421, 0., 0.627 O, -0.699, 0., 1.586 O, 1.888, 0., 0.775	95.64863 8.59957 7.89018	389.5170 1072.3812 1316.7849	-572

[a] Calculated at the B3LYP/aug-cc-pVQZ level of theory. [b] Energy with respect to $P(^4S) + O_2$

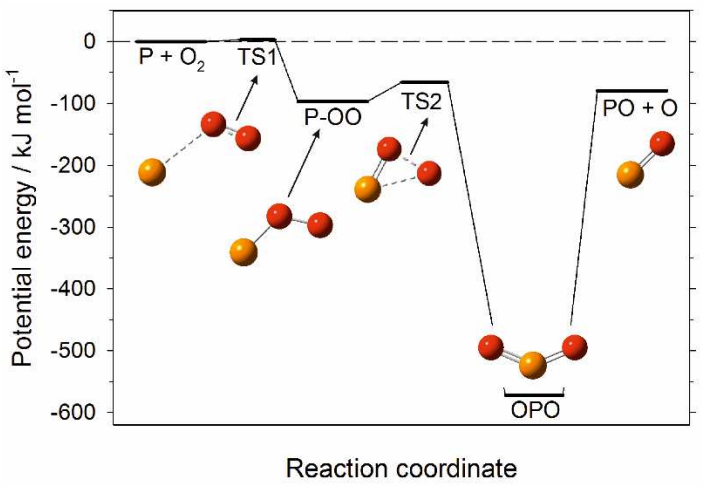

Figure 7. Potential energy surface for the P(^{4}S) + O_2 reaction (doublet spin multiplicity), calculated at the b3lyp/aug-cc-pVQZ level of theory. Atom colours: oxygen (red); phosphorus (yellow).

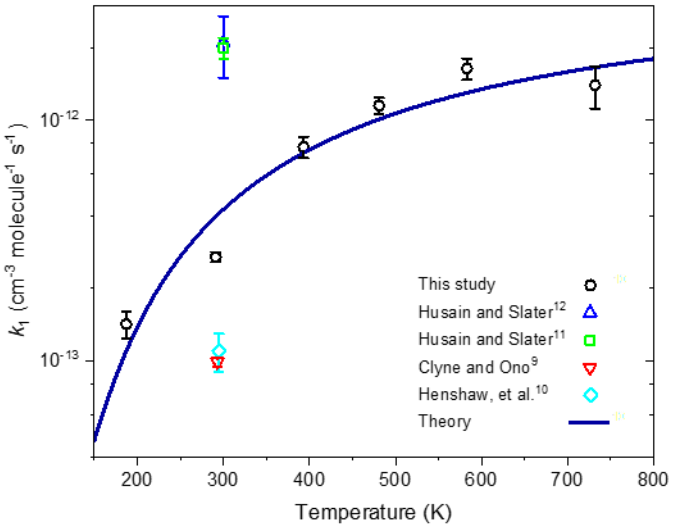

Figure 8. Temperature dependence of the P(^{4}S) + O_2 reaction - comparison of RRKM theory with experiment. Open symbols experimental data from: This study (black circles); Husain and Slater[12] (blue upward facing triangle); Husain and Norris[11] (green square); Clyne and Ono[9] (red downward facing triangle); Henshaw, et al.[10] (turquoise diamond). RRKM theory solid navy line.

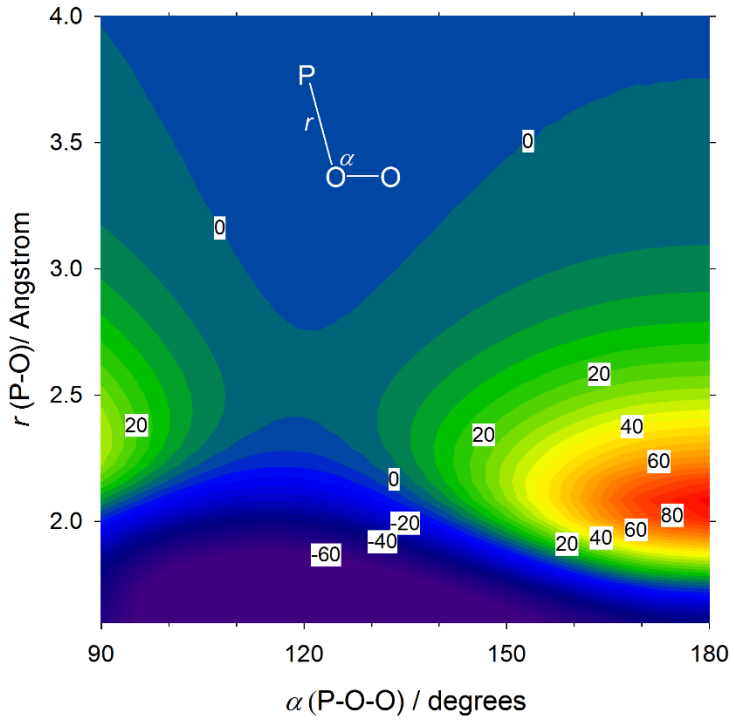

Figure 9. Potential energy surface of doublet spin multiplicity for the P(^{4}S) + O_2 reaction, calculated at the B3LYP/6-311+g(2d,p) level of theory.

5. Conclusions

The reactions of the ground and the first two excited states of phosphorus (the P(^{4}S), P(^{2}D), and P(^{2}P) states, respectively) with atmospherically relevant species have been investigated using the PLP-LIF technique, with the temperature dependence of the reactions being reported for the first time. For the reaction of ground state P(^{4}S) with O_2 (reaction R1) there is significant discrepancy in the literature value reported for k_1 at room temperature, with values varying by around a factor of 20. We have determined a room temperature rate constant towards the lower end of the literature values, with $k_1 = (2.70 \pm 0.12) \times 10^{-13}$ cm^3 molecule^{-1} s^{-1}. The unusual temperature dependence of R1 has also been explained using electronic structure theory combined with RRKM calculations. The small pre-exponential factor for the reaction results from a tight steric constraint, together with the requirement that the reaction occurs on doublet rather than sextet electronic surfaces.

Supporting Information

Additional details regarding the experimental conditions employed in each rate coefficient determination are presented in Tables S1 – S5 of the Supporting Information (SI).

Acknowledgements

This study was supported by funding from the UK Science and Technology Facilities Council (grant ST/P000517/1).

References

1. Maciá, E. The role of phosphorus in chemical evolution. Chem. Soc. Rev. **2005,** 34, 691-701.

2. Redfield, A. C. The biological control of chemical factors in the environment. Am. Sci. **1958,** 46, 205-221.

3. Pasek, M. A. Rethinking early Earth phosphorus geochemistry. P. Natl. A. Sci. **2008,** 105, 853-858.

4. Lodders, K. Solar system abundances and condensation temperatures of the elements. Astrophys. J. **2003,** 591, 1220-1247.

5. Carrillo-Sanchez, J. D.; Nesvorny, D.; Pokorny, P.; Janches, D.; Plane, J. M. C. Sources of cosmic dust in the Earth's atmosphere. Geophysical Research Letters **2016,** 43, 11979-11986.

6. Plane, J. M. C.; Flynn, G. J.; Määttänen, A.; Moores, J. E.; Poppe, A. R.; Carrillo-Sanchez, J. D.; Listowski, C. Impacts of cosmic dust on planetary atmospheres and surfaces. Space Sci. Rev. **2017,** 214, 23.

7. Frisch, M. J.; Trucks, G. W.; Schlegel, H. B.; Scuseria, G. E.; Robb, M. A.; Cheeseman, J. R.; Scalmani, G.; Barone, V.; Petersson, G. A.; Nakatsuji, H., et al. Gaussian 16 Rev. B.01, Wallingford, CT, 2016.

8. Aleksandrov, E. N.; Arutyunov, V. S.; Dubrovina, I. V.; Kozlov, S. N. On the role of PO radicals in the reaction of phosphorus oxidation. Dokl. Akad. Nauk. SSSR **1982,** 267, 110-113.

9. Clyne, M. A. A.;Ono, Y. Kinetic studies of ground-state phosphorus atoms. J. Chem. Soc. Farad. T. 2 **1982,** 78, 1149-1164.

10. Henshaw, T. L.; MacDonald, M. A.; Stedman, D. H.; Coombe, R. D. The $P(^4S_u)$ + $N_3(^2\Pi_g)$ reaction: chemical generation of a new metastable state of PN. J. Phys. Chem. **1987,** 91, 2838-2842.

11. Husain, D.;Norris, P. E. Reactions of phosphorus atoms, $P(3^4S_{3/2})$, studied by attenuation of atomic resonance radiation in vacuum ultraviolet. J. Chem. Soc. Farad. T. 2 **1977,** 73, 1107-1115.

12. Husain, D.;Slater, N. K. H. Time-resolved resonance fluorescence studies of ground state phosphorus atoms, $P[3p^3(^4S_{3/2})]$. J. Chem. Soc. Farad. T. 2 **1978,** 74, 1627-1643.

13. Long, S. R.; Christesen, S. D.; Force, A. P.; Bernstein, J. S. Rate constant for the reaction of PO radical with oxygen. J. Chem. Phys. **1986,** 84, 5965-5966.

14. Sausa, R. C.; Miziolek, A. W.; Long, S. R. State distributions, quenching, and reaction of the PO radical generated in Excimer laser photofragmentation of dimethyl methylphosphonate. J. Phys. Chem. **1986,** 90, 3994-3998.

15. Wong, K. N.; Anderson, W. R.; Kotlar, A. J.; Dewilde, M. A.; Decker, L. J. Lifetimes and quenching of the B $^2\Sigma^+$ PO by atmospheric gases. J. Chem. Phys. **1986,** 84, 81-90.

16. Gobrecht, D.; Cherchneff, I.; Sarangi, A.; Plane, J. M. C.; Bromley, S. T. Dust formation in the oxygen-rich AGB star IK Tauri. Astronomy & Astrophysics **2016,** 585, A6.

17. Mangan, T. P.; McAdam, N.; Daly, S. M.; Plane, J. M. C. Kinetic study of Ni and NiO reactions pertinent to the Earth's upper atmosphere. J. Phys. Chem. A **2019,** 123, 601-610.

18. Gómez Martín, J. C.; Blitz, M. A.; Plane, J. M. C. Kinetic studies of atmospherically relevant silicon chemistry Part I: Silicon atom reactions. Phys. Chem. Chem. Phys. **2009,** 11, 671-678.

19. Acuna, A. U.; Husain, D.; Wiesenfeld, J. R. Kinetic study of electronically excited phosphorus atoms, P(3 ^3D_J, 3 ^2P_J), by atoic-absorption spectroscopy. J. Chem. Phys. **1973,** 58, 494-499.

20. Acuna, A. U.; Husain, D.; Wiesenfeld, J. R. Kinetic study of electronically excited phosphorus atoms, P(3 ^3D_J, 3 ^2P_J), by atoic-absorption spectroscopy. II. J. Chem. Phys. **1973,** 58, 5272-5279.

21. Woon, D. E.;Dunning, T. H. Gaussian-basis sets for use in correlated molecular calculations. III. The atoms aluminium through argon. J. Chem. Phys. **1993,** 98, 1358-1371.

22. Glowacki, D. R.; Liang, C. H.; Morley, C.; Pilling, M. J.; Robertson, S. H. MESMER: An open-source master equation solver for multi-energy well reactions. J. Phys. Chem. A **2012,** 116, 9545-9560.

23. Gilbert, R. G.;Smith, S. C. Theory of Unimolecular and Recombination Reactions. Blackwell: Oxford, 1990.

24. Anicich, V. G. Evaluated bimolecular ion-molecule gas phase kinetics of positive ions for use in modeling planetary atmospheres, cometary comae, and interstellar clouds. J. Phys. Chem. Ref. Data **1993,** 22, 1469-1569.

25. Plane, J. M. C.; Feng, W.; Dawkins, E. C. M. The mesosphere and metals: chemistry and changes. Chem. Rev. **2015,** 115, 4497-4541.

TOC graphic